CCFE
CULHAM CENTRE FOR FUSION ENERGY

UK Atomic Energy Authority

UKAEA-CCFE-PR(20)96

F. Schoofs, F. Ji, A. D. L. Hancock, H. J. Lewtas

Thermodynamic study on steels on the influence of the atmosphere during laser powder bed fusion

Thermodynamic study on steels on the influence of the atmosphere during laser powder bed fusion

F. Schoofs, F. Ji, A. D. L. Hancock, H. J. Lewtas

This is a preprint of a paper submitted for publication in
Journal of Manufacturing and Materials Processing

Thermodynamic study on steels on the influence of the atmosphere during laser powder bed fusion

F. Schoofs[1], F. Ji[2], A. D. L. Hancock[1], H. J. Lewtas[1]

[1]UKAEA - United Kingdom Atomic Energy Authority, Culham Science Centre, Abingdon, OX14 3DB, United Kingdom

[2] Materials Processing Institute, Eston Road, Middlesbrough, TS6 6US, United Kingdom

The atmosphere in powder-based additive manufacturing influences the level of impurities inside the build volume as well as the phases formed during cooldown. We use a thermodynamic model to investigate trends for steels commonly considered for fusion reactors and power plants, namely 316L, F91, F92 and Eurofer97. The atmospheres considered are vacuum (similar to electron beam methods) and gaseous atmospheres based on nitrogen and argon, with impurity levels of 10 and 100 ppm O_2.

1. Introduction

Laser powder bed fusion (LPBF) is an additive manufacturing (AM) technique with the ability to create complex parts with internal structures. Therefore, it has also attracted interest in applications in fusion energy reactors [1], [2]. Typically, the composition of the starting powder is chosen to be what the desired, final, composition of the built part needs to be. This assumes that there is no additional pick-up or loss due to different atmospheres during the AM build phase. The material composition of the component is, however, crucial for activation [3], material behaviour and the related nuclear regulation. The composition will also affect the solidification behaviour and the resulting microstructure.

In this work, we investigate, through thermodynamic modelling, the influence of the build chamber atmosphere on the as-built composition for a limited number of fusion-relevant steels. This would allow the formulation of build atmosphere conditions for specific alloys, in order to end up with the desired material composition and microstructure.

2. Experimental methods

2.1 Materials

The steels chosen for this study are 316L, F91 and Eurofer97 (or Eurofer for short) [4]. The compositions considered for the modelling input are shown in Table 1. For elements with a concentration range in the alloy specification, a mid-range value was selected. We assume that there is no oxygen in the source material, while in practice the concentration in the powder will depend on the supplier, manufacturing process and storage method [5].

Table 1: Compositions (in wt%) for all materials, used as input to the thermodynamic model.

Material	**Cr**	**Ni**	**Mo**	**Mn**	**V**	**Nb**	**W**	**Ta**	**Si**	**P**	**S**	**C**	**N**	**O**
316L	18	10	2.5	0.45	-	-	-	-	0.5	0.03	0.015	0.03	0.1	-
F91	9	0.4	1.0	0.45	0.22	0.08	-	-	0.35	0.02	0.01	0.1	0.07	-
Eurofer	9	-	-	0.4	0.2		1.1	0.12	0.05	0.005	0.005	0.11	0.045	<0.01

2.2 LPBF environments

Our thermodynamic models are valid up to 2500 °C, and this is within the reported 1600-2200 °C peak temperature range that has been demonstrated through LPBF experiments and modelling [6]–[11]. In our model, we assume an upper bound of 2000 °C as the peak temperature that the

material observes. We also assume that at this temperature, the melt is in equilibrium with the atmosphere.

The thermodynamic model requires the incorporation of a certain volume fraction of gas, which is related to the porosity of the powder bed and the bed's interaction with the atmosphere above. For loose, random packing of spheres, a void volume fraction of 40-41% is expected [12]. Experiments have established a void fraction of 35-55% for realistic particle size distributions [13] and models use a fixed 30% [8] or 40% [9]. For our thermodynamic calculations, we use a fixed gas fraction of 40%.

Finally, we consider 4 different atmosphere compositions, which are listed in Table 2. They are a combination of different oxygen, nitrogen and (inert) argon pressures, as well as vacuum. The latter is most applicable to an electron-beam powder bed system, although some sub-atmospheric deposition has also been performed with an LPBF setup [14]. Typical LPBF systems operate in Ar pressures, with oxygen controlled to below 1000 ppm or even below 100 ppm [15].

Table 2: Overview of different atmosphere conditions used in the thermodynamic model.

Atmosphere descriptor	**Pressure**	**O_2**	**N_2**	**Ar**	**He**
N_2 + 100 ppm O_2	1 atm	100 ppm	balance	-	-
Ar + 10 ppm O_2	1 atm	10 ppm	-	balance	-
Ar + 100 ppm O_2	1 atm	100 ppm	-	balance	-
Vacuum	$4 \cdot 10^{-3}$ mbar	-	-	-	$4 \cdot 10^{-3}$ mbar

2.3 Thermodynamic modelling

The thermodynamic software package FactSage 7.3 was used for the modelling. A combination of pure substances, oxides and steel alloy databases were used for performing the modelling calculations. All modelling was based on 100 g of alloy and the extracted data can be found in Ref. [16].

The thermodynamic model does not include any kinetic information. This means that the speed at which the stable phases are formed is unknown. However, the thermodynamic calculations predict the experimental results reasonably well, especially at high temperatures. Within the small amount of material that is quickly melted to high temperatures during the AM process, we expect the phase composition to be close to the model. We used the equilibrium model to estimate the changes in the composition under different temperature, pressure and atmosphere. This model gives equilibrium amounts of phases and composition of liquid, solid and gas phases.

To estimate what phases form during solidification, we used one assumption, namely a Scheil-Gulliver cooling model. This model assumes perfect mobility in the liquid phase, but no changes in the solid phase. Applying this cooling model, allows us to build up a picture of what a solidification composition might look like. The cooling process in LPBF is much faster than the slow cooling assumed here, so more deviation from the model can be expected [17].

3. Results & discussion

3.1. Vacuum conditions

Under the vacuum conditions specified, all elements vaporise quickly after melting. It is, therefore, crucial to keep the heating localised and short, e.g. through the use of electron beams instead of

lasers. Experimentally, it has been found that at these low pressures, the vaporisation of elements indeed starts to affect the quality of the LPBF deposit [14].

3.2 Equilibrium conditions

If we assume that the melt pool is in thermodynamic equilibrium at 2000 °C, we can identify the different phases present in the powder bed at that point. For all materials and atmosphere combinations considered, there is no oxygen-rich slag phase during melting, confirming that the maximum oxygen concentration (from atmosphere and powder combined) can be 100 ppm without creating inclusions.

Figure 1 shows the calculated normalised concentrations of Cr, C and N in the melt at 2000 °C for Ar and N_2-based atmospheres for all steels, as well as the oxygen concentration. The normalisation is done with respect to the starting concentration of each alloy. For all materials and atmospheres, the Cr concentration variation is less 1 % compared to the starting concentration. The carbon concentration is reduced when depositing in atmospheres with 100 ppm O_2, with the 316L material being the most sensitive to this. In both cases, however, the materials remain within their specification.

The nitrogen concentration at equilibrium is elevated for all steels in the N_2 (100 ppm O_2) atmosphere (approximately +10%), but especially for the case of Eurofer melt, which contains over 60% more than the starting content. Based on these values, the 316L and Eurofer LPBF material would be out of specification once solidified. Experimentally a nitrogen increase of ~50 ppm is found in 316L LPBF in nitrogen atmospheres [18], which compares reasonably well to the ~100 ppm estimated from the thermodynamic model. In the Ar atmospheres, almost all starting nitrogen is lost according to the model, yet experimentally the loss appears to be maximum ~20 ppm for 316L [18]. However, the thermodynamic cooling model (section 3.3) shows that the nitrogen concentration in the material increases as it solidifies, which brings the model more in line with the experiment.

The implication is that LPBF would require a tailored Ar atmosphere with carefully chosen N_2 content, if a specific nitrogen concentration in the steel is to be targeted, e.g. to remain within its specification. This N_2 atmosphere content will depend on the type of steel and can be estimated using the thermodynamic model.

The evolution of the equilibrium oxygen concentration (Figure 2) confirms the intuitive expectation that a higher oxygen concentration (100 ppm O_2) results in a higher oxygen pick-up, though the N_2 atmosphere appears to reduce that somewhat. Between the different steels, the 316L melt appears far more sensitive to the oxygen level in the atmosphere, picking up ~10 times more in the 100 ppm O_2 scenario compared to the 10 ppm O_2 scenario.

For a particular alloy and gas mixture, there will be an upper limit to the oxygen concentration in the LPBF atmosphere, beyond which excess oxygen absorption and oxidation occurs, resulting in poorly adhering deposits. For example, for 316L this appears to be above 1000 ppm O_2 in Ar [19]. Even at lower oxygen concentrations, however, oxide layers can form and be incorporated into the deposits [20].

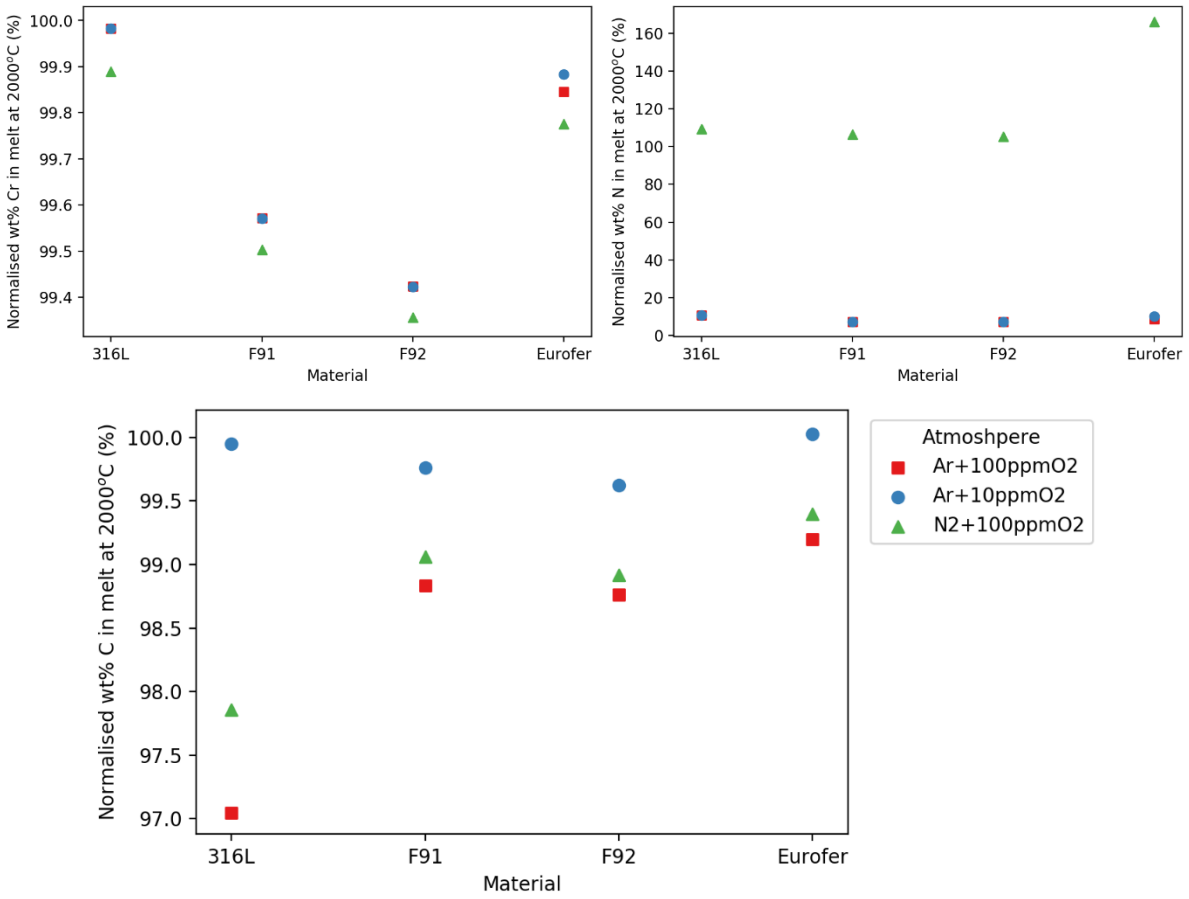

Figure 1: Normalised concentration of Cr, N and C in the liquid metal phase for all steels in different atmospheres.

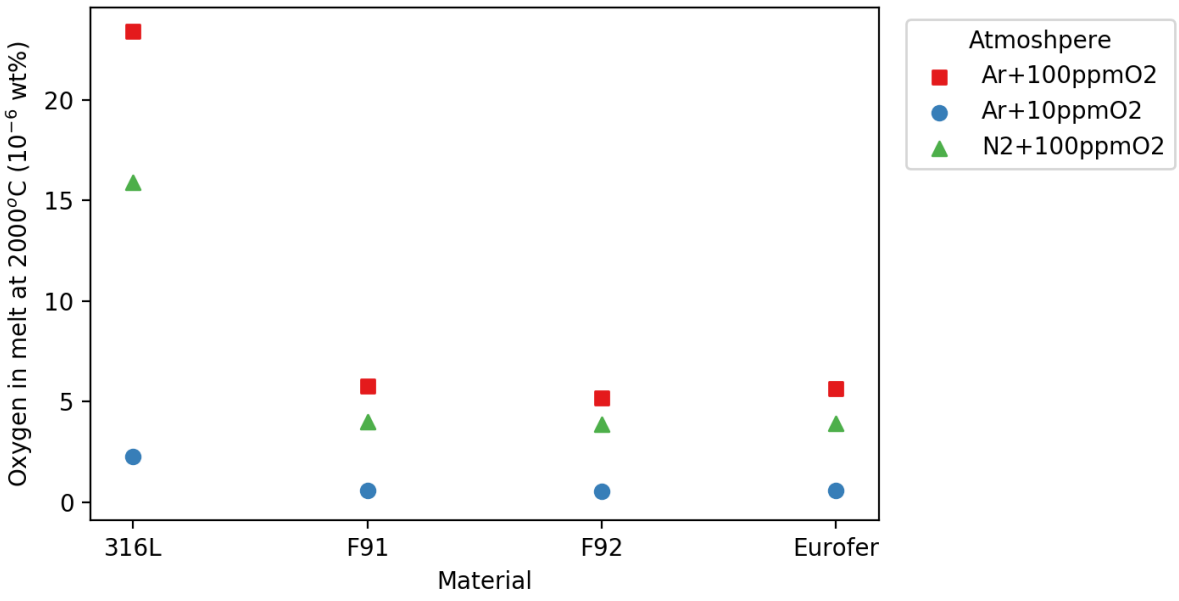

Figure 2: Oxygen concentration in the liquid metal phase of different steels in different LPBF atmospheres.

3.3 Gulliver-Scheil cooling results

Figure 3 shows the Scheil cooling data for 316L for different atmospheres, focusing on the metallic and non-metallic (e.g. carbides and nitrides) phases. The main difference here is between Ar- and N_2-based atmospheres: the nitrogen appears to strongly stabilise the solidification of the FCC

phases as well as result in up to 1 wt% of compound phases. The melt pool also solidifies completely at a higher temperature (~880 °C) compared to an Ar atmosphere (~740 °C). The oxygen content variation in the Ar atmosphere changes very little in 316L. During the solidification process, the Scheil cooling model predicts the formation of SiO_2 and (Mn,Fe) sulphide, which has been experimentally found in 316L deposited under Ar + 100 ppm O_2 [15]. The carbon and nitrogen concentrations in the FCC and BCC phases for different LPBF atmospheres appear to differ only slightly for both Ar atmospheres, whereas it is distinct for the nitrogen atmosphere (Figure 4).

Figures 5 and 6 show the Scheil cooling model data for the metallic and non-metallic phases of F91 steel and Eurofer respectively. As with the case of 316L, the nitride atmosphere has a significantly different behaviour: more and different nitrides are formed earlier in the cooling process. Interestingly, however, is that these two steels exhibit some differences between the two different Ar atmospheres. The BCC vs FCC balance is only subtly changed, but differences are more pronounced when looking at the C and N fractions in these phases (Figures 7 and 8 for F91 and Eurofer respectively). Especially Eurofer appears to differ in the minority FCC equilibrium phase, which will affect its transformation upon cooling and thus the mechanical properties.

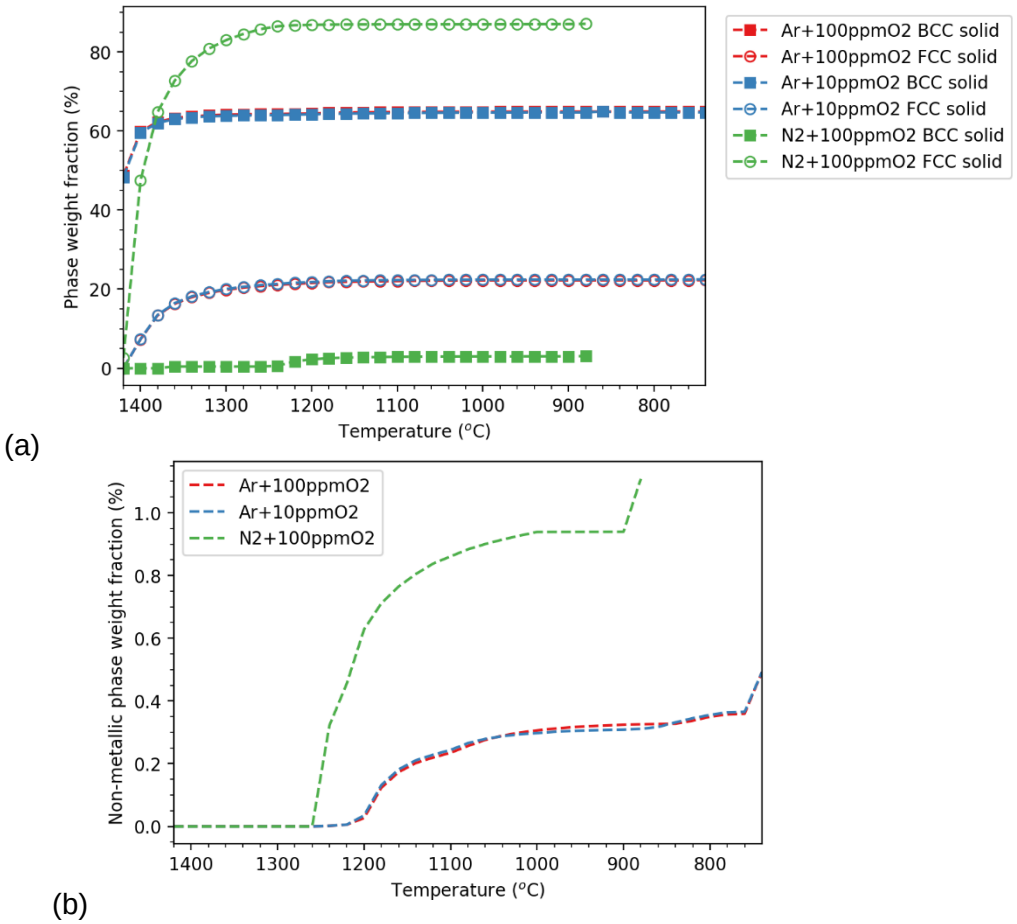

Figure 3: Scheil cooling model data for (a) FCC and BCC metallic phases and (b) non-metallic compounds in 316L for different LPBF atmospheres.

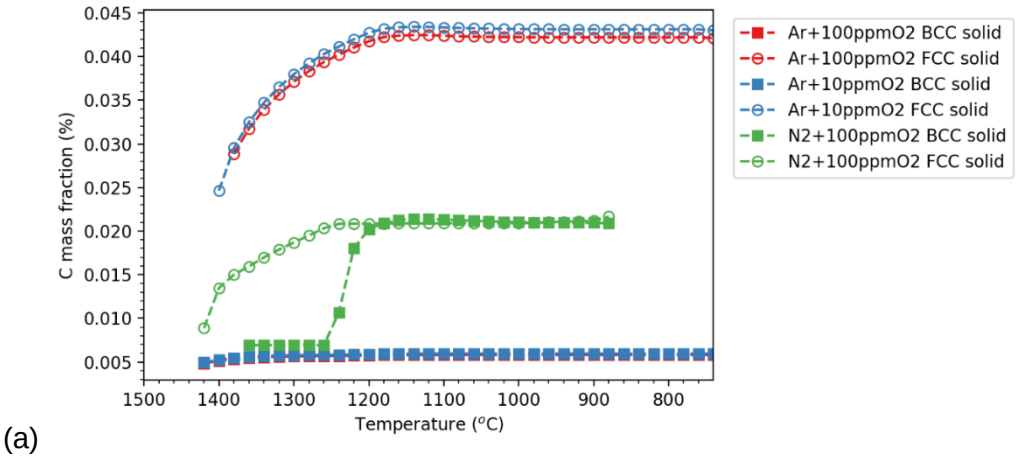

(a)

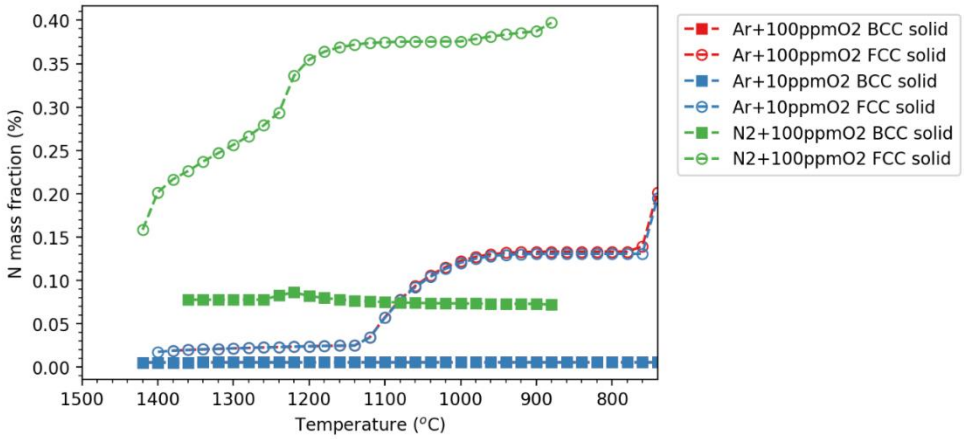

(b)

Figure 4: Scheil cooling model data for (a) C and (b) N mass fraction in the metallic FCC and BCC phases of 316L for different LPBF atmospheres.

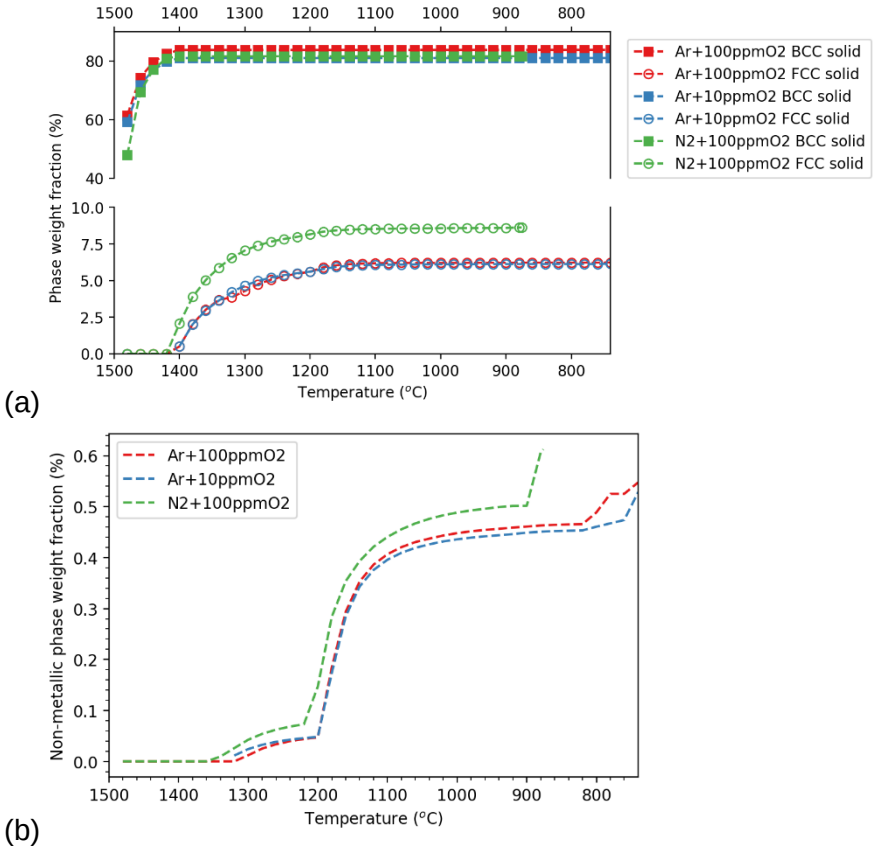

Figure 5: Scheil cooling model data for (a) FCC and BCC metallic phases and (b) non-metallic compounds in F91 for different LPBF atmospheres.

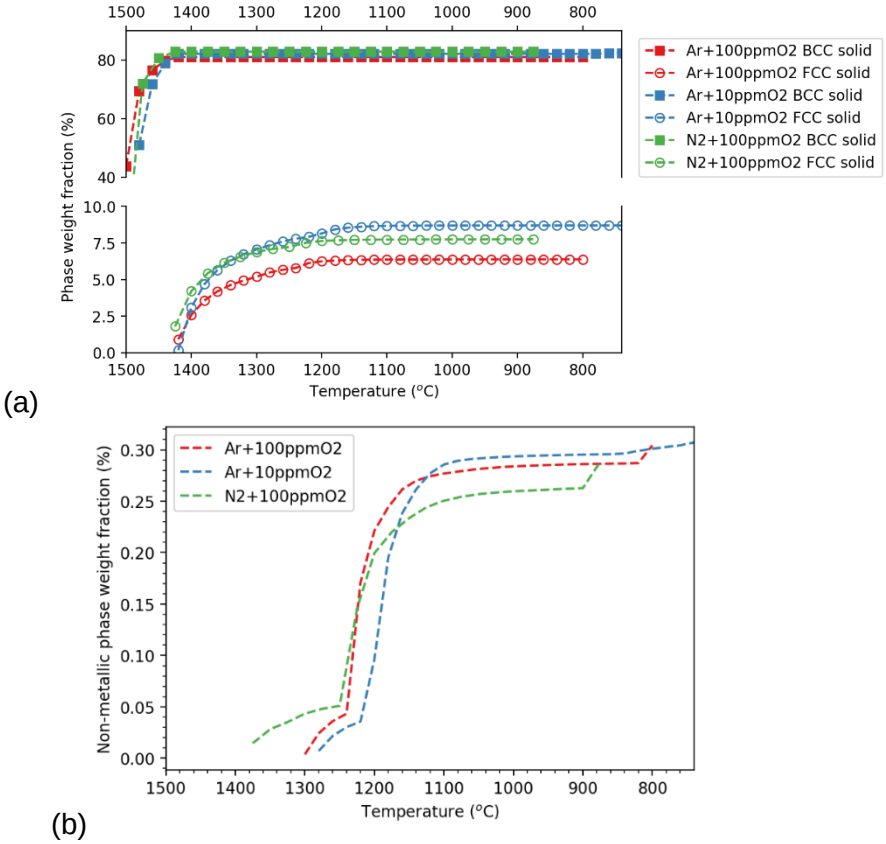

Figure 6: Scheil cooling model data for (a) C and (b) N mass fraction in the metallic FCC and BCC phases of 316L for different LPBF atmospheres

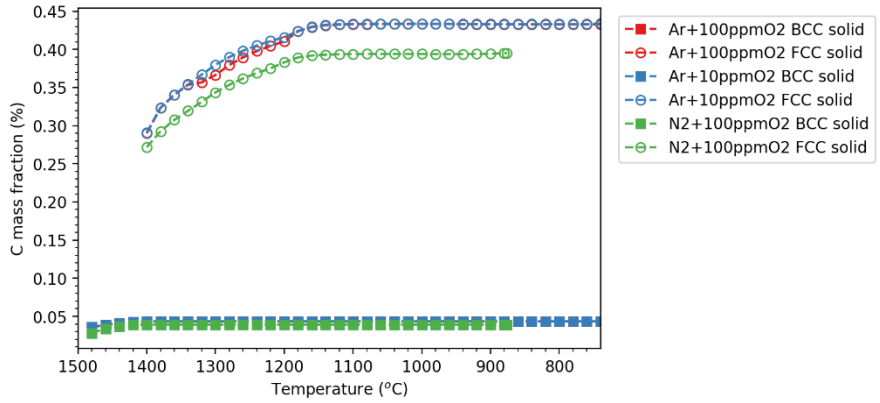

(a)

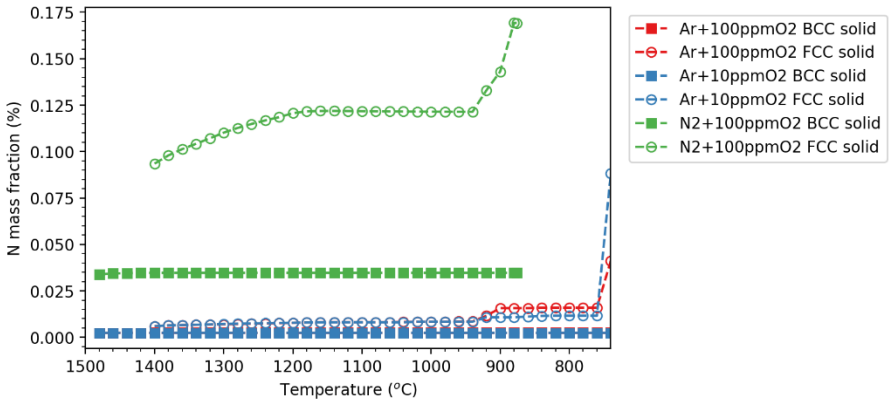

(b)

Figure 7: Scheil cooling model data for (a) C and (b) N mass fraction in the metallic FCC and BCC phases of F91 for different LPBF atmospheres.

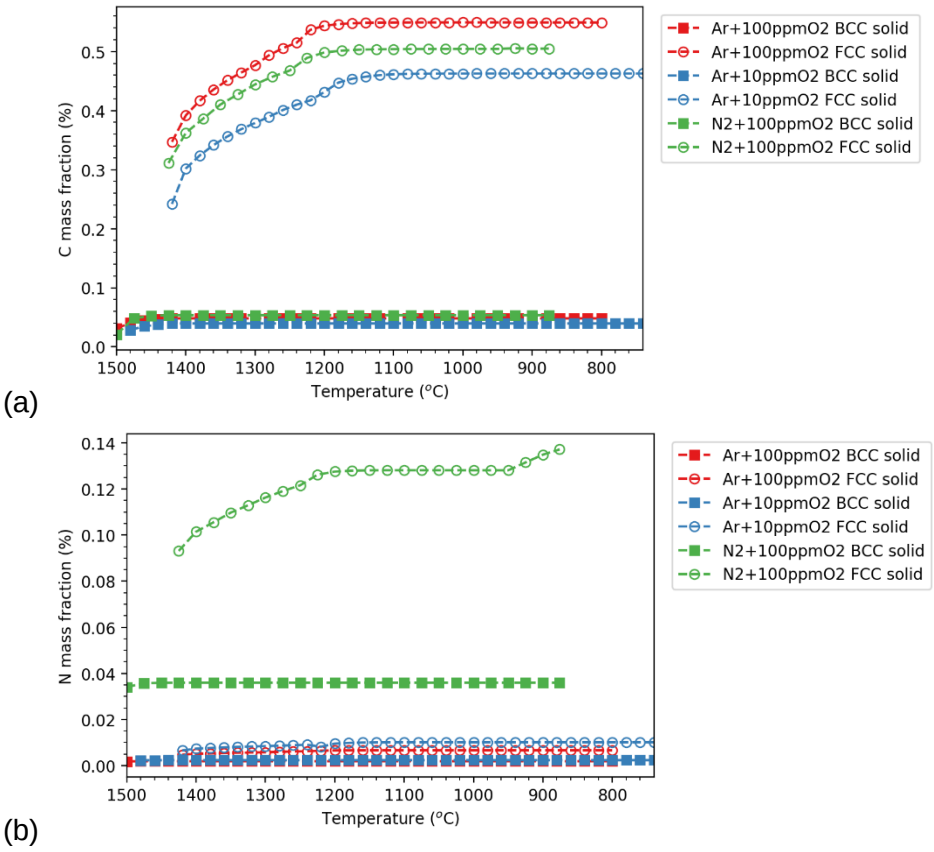

Figure 8: Scheil cooling model data for (a) C and (b) N mass fraction in the metallic FCC and BCC phases of Eurofer for different LPBF atmospheres.

4. Conclusions

The phase composition and cooling behaviour of different steels in different LPBF atmospheres were assessed with thermodynamic calculations. While they cannot represent the nonequilibrium processes during AM, they are able to indicate the direction in which the materials will evolve, depending on the atmosphere. Careful oxygen and nitrogen control, included in the powder itself, is needed to tailor the microstructure and final composition, especially if the latter needs to be within a specific band for regulatory or radioactive waste management reasons. This opens up the possibility of tailored composition powders and/or atmospheres for AM of specific alloys.

Acknowledgements

This work has been funded by the UK Government Department for Business, Energy & Industrial Strategy. To obtain further information on the data and models underlying this paper please contact PublicationsManager@ukaea.uk. F.S. would like to thank Gareth Fletcher for the initial discussions which led to this work.

References

[1] H. Neuberger *et al.*, 'Selective laser sintering as manufacturing process for the realization of complex nuclear fusion and high heat flux components', *Fusion Sci. Technol.*, vol. 72, no. 4, pp. 667–672, 2017.

[2] D. Hancock, D. Homfray, M. Porton, I. Todd, and B. Wynne, 'Exploring complex high heat flux geometries for fusion applications enabled by additive manufacturing', *Fusion Eng. Des.*, vol. 136, no. February, pp. 454–460, 2018.

[3] G. W. Bailey, M. R. Gilbert, and O. Vilkhivskaya, 'Waste Classification Assessment of Nuclear Steels for Fusion Power Applications', in *PHYSOR 2020: Transition to a Scalable Nuclear Future*, 2020.

[4] D. Stork *et al.*, ‘Developing structural, high-heat flux and plasma facing materials for a near-term DEMO fusion power plant: The EU assessment’, *J. Nucl. Mater.*, vol. 455, no. 1–3, pp. 277–291, 2014.

[5] J. Dawes, R. Bowerman, and R. Trepleton, ‘Introduction to the additive manufacturing powder metallurgy supply chain’, *Johnson Matthey Technol. Rev.*, vol. 59, no. 3, pp. 243–256, 2015.

[6] C. Meier, R. W. Penny, Y. Zou, J. S. Gibbs, and A. J. Hart, ‘Thermophysical Phenomena in Metal Additive Manufacturing by Selective Laser Melting: Fundamentals, Modeling, Simulation and Experimentation’, *Annu. Rev. Heat Transf.*, vol. 20, pp. 241–316, 2017.

[7] E. Mirkoohi, J. Ning, P. Bocchini, O. Fergani, K.-N. Chiang, and S. Liang, ‘Thermal Modeling of Temperature Distribution in Metal Additive Manufacturing Considering Effects of Build Layers, Latent Heat, and Temperature-Sensitivity of Material Properties’, *J. Manuf. Mater. Process.*, vol. 2, no. 3, p. 63, 2018.

[8] A. Hussein, L. Hao, C. Yan, and R. Everson, ‘Finite element simulation of the temperature and stress fields in single layers built without-support in selective laser melting’, *Mater. Des.*, vol. 52, pp. 638–647, 2013.

[9] R. Andreotta, L. Ladani, and W. Brindley, ‘Finite element simulation of laser additive melting and solidification of Inconel 718 with experimentally tested thermal properties’, *Finite Elem. Anal. Des.*, vol. 135, no. July, pp. 36–43, 2017.

[10] T. Loewenhoff *et al.*, ‘Impact of combined transient plasma/heat loads on tungsten performance below and above recrystallization temperature’, *Nucl. Fusion*, vol. 55, no. 12, p. 123004, Nov. 2015.

[11] J. Ning, D. E. Sievers, H. Garmestani, and S. Y. Liang, ‘Analytical Thermal Modeling of Metal Additive Manufacturing by Heat Sink Solution’, *Materials (Basel).*, vol. 12, no. 16, p. 2568, 2019.

[12] F. A. L. Dullien, *Porous Media: Fluid Transport and Pore Structure*, 2nd ed. 1991.

[13] U. Ali *et al.*, ‘On the measurement of relative powder-bed compaction density in powder-bed additive manufacturing processes’, *Mater. Des.*, vol. 155, pp. 495–501, 2018.

[14] P. Bidare, I. Bitharas, R. M. Ward, M. M. Attallah, and A. J. Moore, ‘Laser powder bed fusion at sub-atmospheric pressures’, *Int. J. Mach. Tools Manuf.*, vol. 130–131, pp. 65–72, 2018.

[15] A.-H. Puichaud *et al.*, ‘Microstructure and mechanical properties of 316L stainless steel produced by selective laser melting’, *EPJ Nucl. Sci. Technol.*, vol. 5, p. 23, 2019.

[16] F. Schoofs, ‘Thermodynamic modelling data for LPBF of 316L, F91, F92, Eurofer97’, 2020. [Online]. Available: https://doi.org/10.6084/m9.figshare.12356423.

[17] W. Li, X. Chen, L. Yan, J. Zhang, X. Zhang, and F. Liou, ‘Additive manufacturing of a new Fe-Cr-Ni alloy with gradually changing compositions with elemental powder mixes and thermodynamic calculation’, *Int. J. Adv. Manuf. Technol.*, vol. 95, pp. 1013–1023, 2018.

[18] C. Pauzon, E. Hryha, P. Forêt, and L. Nyborg, ‘Effect of argon and nitrogen atmospheres on the properties of stainless steel 316 L parts produced by laser-powder bed fusion’, *Mater. Des.*, vol. 179, p. 107873, 2019.

[19] R. Li, J. Liu, Y. Shi, L. Wang, and W. Jiang, ‘Balling behavior of stainless steel and nickel powder during selective laser melting process’, *Int. J. Adv. Manuf. Technol.*, vol. 59, no. 9–12, pp. 1025–1035, 2012.

[20] A. T. Sutton, C. S. Kriewall, M. C. Leu, J. W. Newkirk, and B. Brown, ‘Characterization of laser spatter and condensate generated during the selective laser melting of 304L stainless steel powder’, *Addit. Manuf.*, vol. 31, no. September 2019, p. 100904, 2020.